45th AIAA Aerospace Sciences Meeting and Exhibit
8 - 11 January 2007, Reno, Nevada

AIAA 2007-1272

45th AIAA Aerospace Sciences Meeting and Exhibit, Jan 8-11, 2007 Reno, NV

Aerodynamic Characteristics of Slender Delta Wing with Low Dorsal Fin

Xuanshi Meng*, Chun Jia†, Zhide Qiao‡, Chao Gao§
Aerodynamic Design and Research National Laboratory
Northwestern Polytechnical University, Xi'an 710072, China
Shijun Luo¶ and Feng Liu‖
Department of Mechanical and Aerospace Engineering
University of California, Irvine, CA 92697-3975

Cai, Liu, and Luo developed a vortex stability theory (J. of Fluid Mech., vol. 480, 2003, pp. 65-94) for slender conical bodies and predicted that vortices over a flat-plate delta wing at high angles of attack with zero sideslip were conical, symmetric, and stable but adding a low dorsal fin to the wing would destabilize the vortices and therefore render the originally symmetric vortices asymmetric. The wing is assumed slender so that no vortex breakdown occurs on the wing. An experimental study using a six-component internal strain-gage balance is conducted to verify the validity of the theoretical predictions and shows the force development versus angle of attack. A sharp-edged flat-plate delta wing of 82.5° sweep angle is tested in a low-speed wind tunnel at angles of attack up to 32° and sideslip within $\pm 10^\circ$. The same tests are performed on an identical delta wing model but with a low dorsal fin mounted vertically in the incidence plane of the wing. Two fin heights are tested. The ratios of the local fin height to the local wing semi-span are 0.3 and 0.6. The measurement of the aerodynamic forces and moments clearly indicates that a force-asymmetry onset occurs over the wing-fin models at zero sideslip, providing for the first time force measurement evidence of the theoretical predictions and depicts that the force-asymmetry onset can be followed by a force-unsteadiness onset.

Nomenclature

b	=	wing span
c_r	=	root chord
$\bar{c}$	=	mean aerodynamic chord of wing
C_D	=	drag coefficient, $D/q_\infty S$
C_L	=	lift coefficient, $L/q_\infty S$
C_l	=	rolling-moment coefficient, $M_X/q_\infty Sb$
C_m	=	pitching-moment coefficient, $M/q_\infty S\bar{c}$
C_N	=	normal force coefficient, $-F_z/q_\infty S$
C_n	=	yawing-moment coefficient, $M_Z/q_\infty Sb$
C_T	=	tangential force coefficient, $-F_X/q_\infty S$
C_Y	=	side-force coefficient, $F_Y/q_\infty S$
D	=	drag referred to wind axes

*Graduate Student.
†Graduate Student.
‡Professor.
§Professor.
¶Researcher.
‖Professor. Associate Fellow AIAA.

$-F_X$	=	tangential force referred to balance body axes
F_Y	=	side force referred to balance axes and wind axes
$-F_Z$	=	normal force referred to balance body axes
h	=	fin height
K	=	Sychev similarity parameter, $\tan\alpha/\tan\epsilon$
K_S	=	$\tan\beta/\sin\alpha$
L	=	lift referred to wind axes
M	=	pitching moment about wind axes, origin at 40% $\bar{c}$
M_X	=	rolling moment about X-axis
M_Y	=	pitching moment about Y-axis
M_Z	=	yawing moment about Z-axis
q_∞	=	free-stream dynamic pressure
S	=	wing area
s	=	wing semi-span
U_∞	=	free-stream velocity
X, Y, Z	=	balance body axes
α	=	angle of attack
β	=	angle of sideslip
ΔC_l	=	increment of C_l
ΔC_n	=	increment of C_n
ΔC_Y	=	increment of C_Y
ϵ	=	half vertex angle of wing
κ_l	=	dimensionless rolling-moment arm based on b
κ_n	=	dimensionless yawing-moment arm based on b

I. Introduction

Symmetric separation vortices over slender bodies may become asymmetric as the angle of attack is increased beyond a certain value, causing asymmetric forces even at symmetric flight conditions. The transition of the vortex pattern from being symmetric to asymmetric over symmetric bodies under symmetric flow conditions is a fascinating fluid dynamics problem and of major importance for the performance and control of high-maneuverability flight vehicles that favor the use of slender bodies. Excellent reviews on this subject can be found in the papers by Ericsson,[1] and Lowson and Ponton.[2]

Shanks[3] (1963) performed tests of a series of thin flat-plate delta wings having leading-edge sweep angles of 70 degrees to 84 degrees and found in the variation of the lateral three-components with angle of sideslip for various angles of attack, the curves for the 82 degrees and 84 degrees sweep wings became asymmetric about zero sideslip with increase in angle of attack. Shanks' experiment led to the belief that the vortex flow over a low aspect-ratio delta wing with sharp leading-edges, like the flow over slender pointed bodies of revolution, would become asymmetry at high angles of attack and zero sideslip before vortex breakdown occurs over the wing. (See, for example, Polhamus[4] and Keener and Chapman.[5]) Later, Stahl, Mahmood, and Asghar[6] (1992) performed water tunnel and wind tunnel experiments and concluded based on their flow visualization that the vortex flow over slender delta wings with sharp leading edges remained symmetric at all angles of attack until vortex breakdown occurred on the wing. That conclusion, which is now generally accepted, seemingly contradicted the observations by Shanks. Ericsson[1](1992), however, noticed that Shanks' wing model differed from that by Stahl et al. in that Shanks' model contained a low center spline or 'fuselage bump' on the lee-side of the wing. Ericsson claimed that the vortex asymmetry observed in Shanks' experiment was not due to hydrodynamic instability but rather likely due to asymmetric re-attachment in the presence of the centerline spline.

Cai, Liu, and Luo[7] developed a vortex stability theory for slender conical bodies and showed by their analytical methods that vortices over a flat-plate delta wing at zero sideslip are conical, symmetric, and stable for all angles of attack but adding a low dorsal fin to the wing would destabilize the vortices and

therefore render the originally symmetric vortices asymmetric, non-conical, and probably, unsteady. The forward half of the Shanks' models approximated conical bodies. By examining the data in Shanks test and comparing with their predicted range of fin heights needed to destabilize the vortex flow, Cai, et al.[7] suggested that the vortex asymmetries observed in Shanks experiments were caused by the destabilizing effect of the center spline, which functions as a low height dorsal fin on Shanks' flat-plate delta wings.

It may be argued that the 'bump' on Shanks' test model is not exactly a flat-plate fin as assumed in the theory by Cai et al.[7] Meng et al.[8] designed a strictly slender and conical flat-plate fins of different heights and added to a sharp-edged flat-plate delta wing and used a smoke-laser-sheet visualization technique to visualize and measure the positions of the vortex pair over the delta wing with and without fins at an angle of attack of 29.02 degrees and zero sideslip. The observation showed that the symmetric and conical vortex pair over the wing remains stationary when the dorsal is high, but becomes asymmetric, non-conical and unsteady for the wing with a low fin, which confirms the instability predictions of Ref. 7.

It is obvious that if the dorsal fin added into the symmetry plane of a wing is high enough, the stationary symmetric vortex pair over the original wing will not change. But the change brought about by the fin of low height needs more careful investigation. The purpose of this work is to study the unusual change by measuring the six components of the aerodynamic force and moment acting on a slender flat-plate delta wing with low dorsal fins of different heights. Moreover, the visualization study of Ref. 8 was limited to an extremely small wind speed ($Re = 2.99 \times 10^5$). In the force measurement study this restriction is removed.

In the following sections, the stability theory of Ref. 7 is briefly reviewed and the theoretical results for the experimental cases are presented. The details of the experimental setup for the measurement of the forces and moments are described. The experimental results are then presented, analyzed and compared with the theoretical predictions. Lastly, conclusions are drawen.

II. Theoretical Method

In this section, a brief review of the theoretical vortex-flow model and the stability analysis method developed in Refs. 7 and 9 are presented.

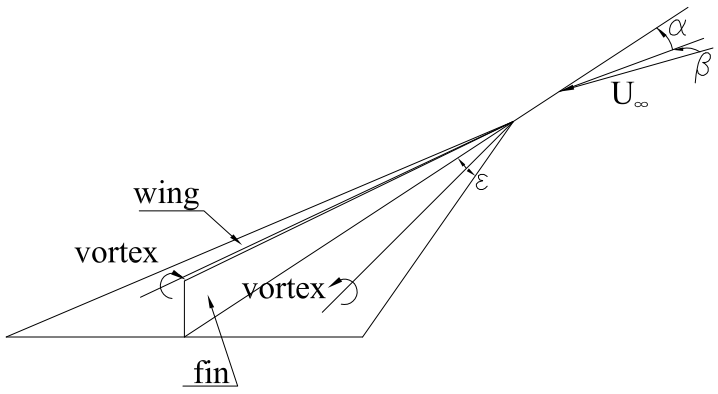

Figure 1. Slender conical wing and low dorsal fin combination and the vortex model.

Consider the flow past a slender conical wing and dorsal fin combination at an angle of attack α and sideslip angle β as shown in Fig. 1. The velocity of the free-stream flow is U_∞. The planform of the wing has a half vertex angle of ϵ. The wing-fin combination is assumed to be conical and of infinite length. No effects of trailing edge are considered. At high angles of attack, there are vortices separated from the sharp leading edges of the wing. To study the stability of the vortex flow, the theoretical model used here is mainly that of Legendre.[10] The vortex model consists of one pair of concentrated vortices separated from the sharp leading edge of the wing as shown in Fig. 1. The distributed vortex sheets that connect the leading edges and the two concentrated vortices are neglected since their strength is in general much smaller than that of the two concentrated vortices. The two concentrated vortices are assumed to be conical rays from the body apex. Secondary separation vortices separated from the wing surface and separated vortex from the leading edge of the fin, if any, are weak and thus also neglected. No vortex breakdown occurs on the wing. The flow is assumed to be steady, inviscid, incompressible, conical, and slender.

The inviscid incompressible flow considered in the above model is irrotational except at the lines of the isolated vortices. The governing equation for the velocity potential is the three-dimensional Laplace equation with zero normal flow velocity on smooth body surfaces, and Kutta conditions at sharp leading edges of the wing as boundary conditions. By means of the slender body theory and the conical flow assumption, the problem is reduced to a two-dimensional potential flow in the cross-flow plane. Only vortex configurations (locations and strengths of the vortices) that result in zero flow velocities at the two vortex centers can exist in a steady flow. These locations of the vortices are called the *stationary* positions.

When a vortex pair is slightly perturbed from their *stationary* positions and then released, its motion follows the vortex velocity. The increments of its coordinates as function of time are governed by a system of two linear homogeneous first-order ordinary differential equations. The eigenvalues λ_1 and λ_2 of the system depend on the Sychev similarity parameter K,[11] the sideslip similarity parameter K_S, and the geometric parameter, h/s. Any perturbation of the *stationary* positions of the vortex pair can be decomposed into a symmetric perturbation and an anti-symmetric perturbation. The maximum real part of the two eigenvalues λ_1 and λ_2 for each vortex of the *stationary* vortex pair under small symmetric or anti-symmetric perturbations is used to determine stability in this analysis. A positive value of this variable means perturbation growth (unstable), a negative value means perturbation decay (stable), and a zero value means perturbation remain (neutrally stable). A vortex pair is stable if and only if both vortices are stable under both symmetric and anti-symmetric perturbations. Such an instability is known as absolute instability.

In the original analyses, the separation vortices are modeled by lines of zero diameter with concentrated vortex strength. (See Fig. 1.) However, the real scenario is that the shear layer separated from the wing curves upward and inboard and eventually rolls up forming a core in which flow velocity and vorticity are high and pressure is low. Over a slender conical fore-body, the vortex core is roughly conical and has a diameter as large as one-third of the semi-span of a delta wing. The original theory in Ref. 7 is modified by Cai et al.[9] to account for the effects of the vortex cores. The jet-like flow in the vortex core and inflow at its outer edge are modeled based on numerical experiments by the Euler methods on slender conical bodies incorporated with known theoretical and experimental results on vortex cores. Using the Euler solutions as a benchmark, the modified model yields a better predictions in the vortex positions than the original, and a favorable shifts of the transition point of stability in K, as shown in Ref. 9.

III. Theoretical Results

In the following experiments, a delta wing of a semi-vertex angle, $\epsilon = 7.5^\circ$ with and without a dorsal fin of a height, $h = 0.3s$ or $0.6s$ in the symmetry plane of the wing is considered. The theoretical results for the three experimental models are calculated by the modified theory.[9]

It is obtained that there exists *stationary* symmetric vortex pair over the wing with and without dorsal fin considered at high angles of attack and zero sideslip. The stability of the *stationary* symmetric vortex pair under small symmetric and anti-symmetric perturbations is studied.

Figure 2 presents the maximum real part of the two eigenvalues for the stability of the *stationary* symmetric vortex pair versus angle of attack at zero sideslip for a flat-plate delta wing with a semi-vertex angle, $\epsilon = 7.5^\circ$. Fig. 3 presents the maximum real part of the two eigenvalues for the stability of the *stationary* symmetric vortex pair for the wing with a dorsal fin of heights, $h = 0.3s$ and $0.6s$ at zero sideslip. For the case of wing alone, the *stationary* symmetric vortex pair is stable and the stability curves under symmetric

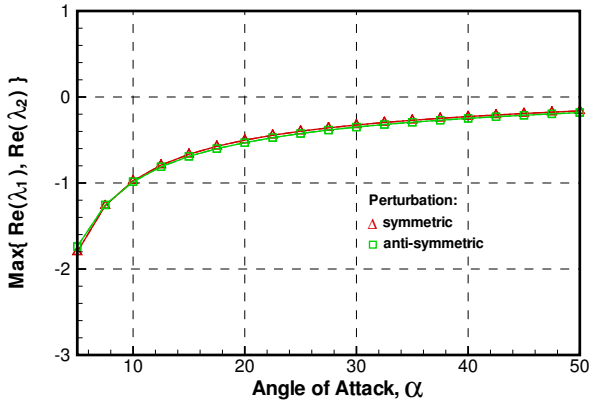

Figure 2. Maximum real part of eigenvalues for stability of the *stationary* symmetric vortex pair vs. α (deg) over a flat-plate delta wing, $\epsilon = 7.5°$, $\beta = 0$.

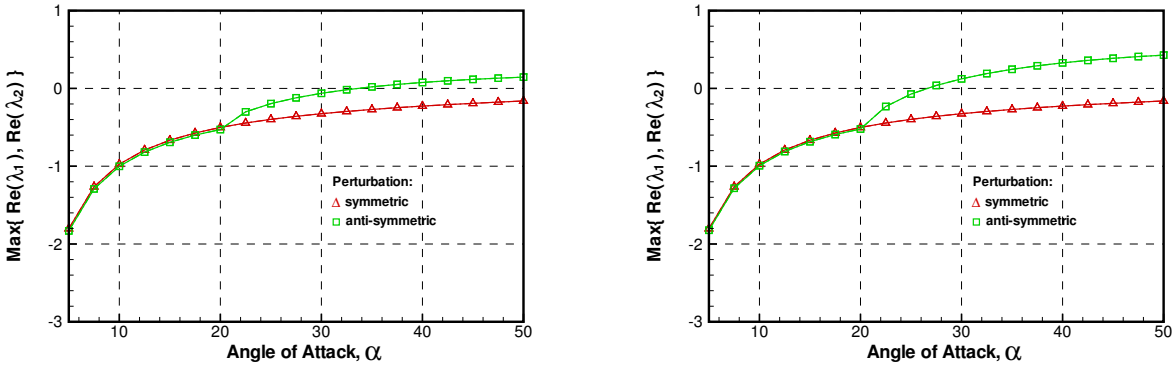

(a) Wing+0.3s-fin model

(b) Wing+0.6s-fin model

Figure 3. Maximum real part of eigenvalues for stability of the *stationary* symmetric vortex pair vs. α (deg), $\epsilon = 7.5°$, $\beta = 0$.

and anti- symmetric perturbations coincide each other. For the two cases of wing-fin combination, the stability curves under symmetric perturbation remain the same as that of the wing alone as it should be, since the the fins are positioned in the symmetry plane of the wing and the perturbation is symmetric. Under anti-symmetric perturbation, the stability curves for the the two wing-fin cases deviate from that of the wing alone. The *stationary* symmetric vortex pair over the wing-fin combination is stable when the angle of attack is low and becomes unstable as the angle of attack is increased beyond certain value. The instability onset occurs at $\alpha = 33.57^\circ$ and 26.72° for $h = 0.3s$ and $0.6s$, respectively.

It is fantastic that a low dorsal fin has a destabilizing effect to the originally stable *stationary* symmetric vortex pair over a slender delta wing, in consideration of that the fin is seated in the symmetry plane of the wing and the sideslip angle is zero. The higher the dorsal fin is, the greater the destabilizing effect will be and, therefore, a lower angle of attack is required for the instability to occur for the higher fin case. The destabilizing effect is caused by the interaction between the vortex pair and the wing with low dorsal fin under small perturbations. Moreover, from Fig. 3 that the destabilizing effect of the low dorsal fin does not appear when the angle of attack is low and it occurs only after the angle of attack is increased beyond 20° for the wing with a semi-vertex angle of 7.5°. (In general, $K > 2.765$.) When $\alpha \leq 20^\circ$, no destabilizing effect of the low dorsal fin appears at all.

A corresponding calculations by the original theory[7] are also conducted, and similar results are obtained. The angle of attack for the instability onset at zero sideslip predicted by the original and modified theory is listed in Table 1, where No denotes no instability onset. The ignorance of the vortex core exaggerates the destabilizing effect of the low dorsal fin.

Table 1 Theoretical angle of attack for instability onset, $\epsilon = 7.5^\circ$, $\beta = 0$.

Model	Original theory[7]	Modified theory[9]
Wing	No	No
Wing+0.3s-fin	22.55°	33.57°
Wing+0.6s-fin	17.85°	26.72°

Furthermore, the theory[12] predicts that unlike the case of a slender circular cone, there exist no *stationary* asymmetric conical vortex solutions for the slender flat-plate delta wing at high angles of attack and zero sideslip. If the *stationary* symmetric conical vortex pair over the combination of slender conical wing and fin becomes unstable, it is most likely asymmetric and non-conical. The present theory of stability is a linear analysis which assumes that the displacement of the *stationary* vortices remains small. Once the displacement becomes large, the linear theory can not tell.

IV. Experimental Setup

Wind tunnel testing problems at high angles of attack mentioned in the literature include flow unsteadiness and model vibrations. The problem of flow unsteadiness is minimized by selecting a wind tunnel of large size and high-quality test-section flow. All the tests of this paper are conducted in the NF-3 wind tunnel at the Aerodynamic Design and Research National Laboratory, Northwestern Polytechnical University. The test section has a width of 3.5 m, a height of 2.5 m, and a length of 12 m. The contraction ratio is $11:1$. The free-stream turbulence level is 0.08% for the wind speeds of $15 \sim 90$ m/s. The variation of the free-stream velocity direction is within $\pm 0.5^\circ$. The variation of the wind speed is within ± 0.5 m/s. The measurement accuracy of α and β is within $\pm 0.09^\circ$.

The model and its support are made carefully to minimize experimental problems. The wing has a sweep angle of 82.5° and root chord of $c_0 = 990.0$ mm. The wing is made of aluminum alloy. In order to have enough longitudinal stiffness, the thickness of 15.0 mm is chosen. The thickness ratio of the root section is 1.5% . It is known that the wing models of Shanks[3] were made of 3.175 mm aluminum alloy. The thickness ratio of the root section of the wing with 82° sweep angle is 0.16%. However, in Shanks' wing model there was a fuselage-shaped fairing (to accommodate the internal balances) having a maximum height of 0.5 semi-span of the wing and made of 0.8 mm aluminum alloy attached to the upper surface of the wing all way along the root chord of the wing which provided longitudinal stiffness to the wing. Different from the Shanks' wing models, the leading and trailing edges of the present wing are all beveled with a 20° angle from the

windward side of the wing so that the leeward side of the wing is perfectly flat. The dorsal fins are made of 2.0 mm aluminum alloy. The leading edge of the fins is sharpened symmetrically with a 45° angle from both sides. Two fin heights are chosen: $h = 0.3s$ and $0.6s$.

The tip portion of all models from the apex to a station of 160.0 mm along the root chord is separately made for construction reasons. The use of the separate tips is to increase the precision in forming an accurate conical nose as assumed the the theory, since it is known that the flow is sensitive to geometric imperfections in the tip region. The tips are made of aluminum alloy. The main portion of the wing after the tips is common to all models. Care was taken to accurately match the tips with the main part of the wing with and without fin. The wing model is shown in Fig. 4. The dorsal fin is fixed vertically on the upper surface of the wing in its symmetry plane. The models are made to very close tolerances and have a high surface finish.

The forces and moments are measured about the balance body axes by a six-component internal strain-gage balance. The balance has a diameter of 36 mm and a length of 230 mm. Because the purpose of this investigation is to determine the force characteristics of the wing and its combinations with dorsal fins, the balance is kept to minimize the aerodynamic influence of the balance to the models. The balance is attached on the lower surface of the wing and very close to the wing trailing edge. The longitudinal axis of the balance is parallel to the root chord of the wing and lies in the symmetry plane of the wing. The center of the balance lies a distance of 36 mm below the upper surface of the wing and the project of the balance center on the wing root chord is located at a distance of 7.5 mm ahead of the trailing edge of the wing. As the wing and balance combination once is setup, it is not changed throughout the entire tests. The fins are fixed in and out without alternating the setup. In consideration of the small size of the balance relative to the test models and its location close to the wing trailing edge, no fairing is implemented to accommodate the balance, except the blunt leading end is covered by a conical plaster to reduce the aerodynamic force on the balance. The internal strain-gage balance is sting mounted rigidly onto the model support of the wind-tunnel test section as shown in Fig. 5.

The six aerodynamic components acting on the model are measured and referred to the balance body coordinate system $OXYZ$. The system origin O is set at the center of the balance. The system axis OX lies in the symmetry plane of the model and parallel to the root chord of the wing pointing upstream. The axis OY is parallel to the wing span direction pointing to the right side of the wing. The axis OZ is normal to the upper surface of the wing pointing downward. The three axes OX, OY, and OZ form a right-hand system as shown in Fig. 5. The three force components along the axes OX, OY, and OZ are the tangential force $-F_X$, side force F_Y and normal force $-F_Z$. The three moment components are the rolling moment M_X, pitching moment M_Y and yawing moment M_Z. The balance coordinate system does not coincide with the wing body system. However, their axes are parallel each other.

The measurement range and the measurement uncertainty of the six-component internal strain-gage balance are shown in Table 2. The uncertainty of the six-component coefficients produced by the balance measurements at the free-stream velocity $U_\infty = 25\ m/s$ and $35\ m/s$ are listed in Table 3. The balance is not specifically designed for the present test. Due to the limitation of its M_Y-measurement range, no test is conducted at higher wind speeds.

Table 2 Measurement range and measurement uncertainty of the six components.

Item	$-F_X, N$	F_Y, N	$-F_Z, N$	$M_X, m-N$	$M_Y, m-N$	$M_Z, m-N$
Range	±392.140	±294.105	±588.210	±24.509	±34.312	±29.411
Uncertainty	±0.9016	±0.6850	±1.0122	±0.0650	±0.1193	±0.1026

Table 3 Measurement uncertainty of the six-component coefficients.

U_∞	C_T	C_Y	C_N	C_l	C_m	C_n
$25\ m/s$	±0.0024	±0.0018	±0.0027	±0.0001	±0.0003	±0.0003
$35\ m/s$	±0.0012	±0.0009	±0.0014	±0.0001	±0.0002	±0.0002

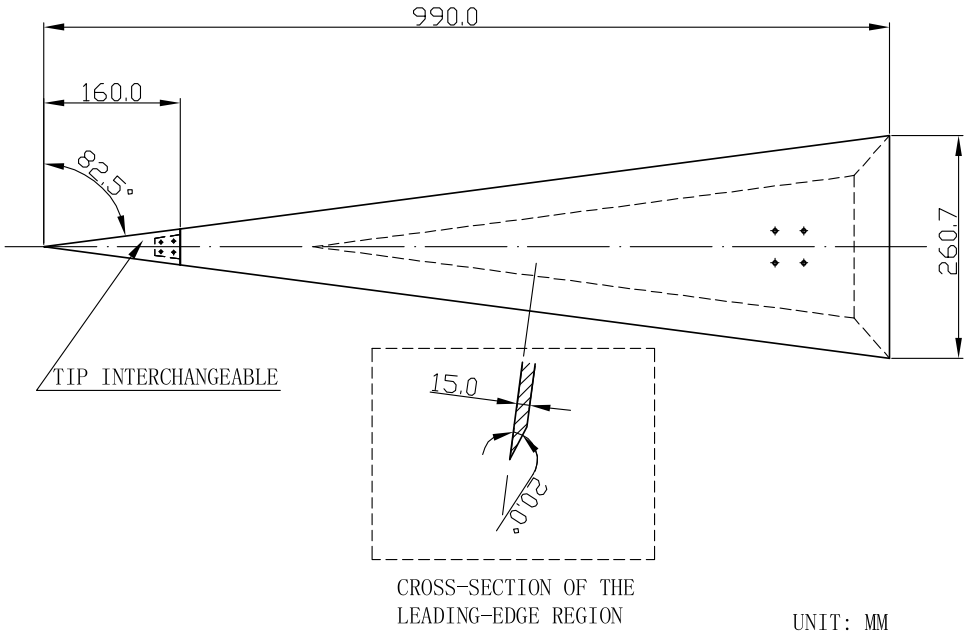

Figure 4. The wing model.

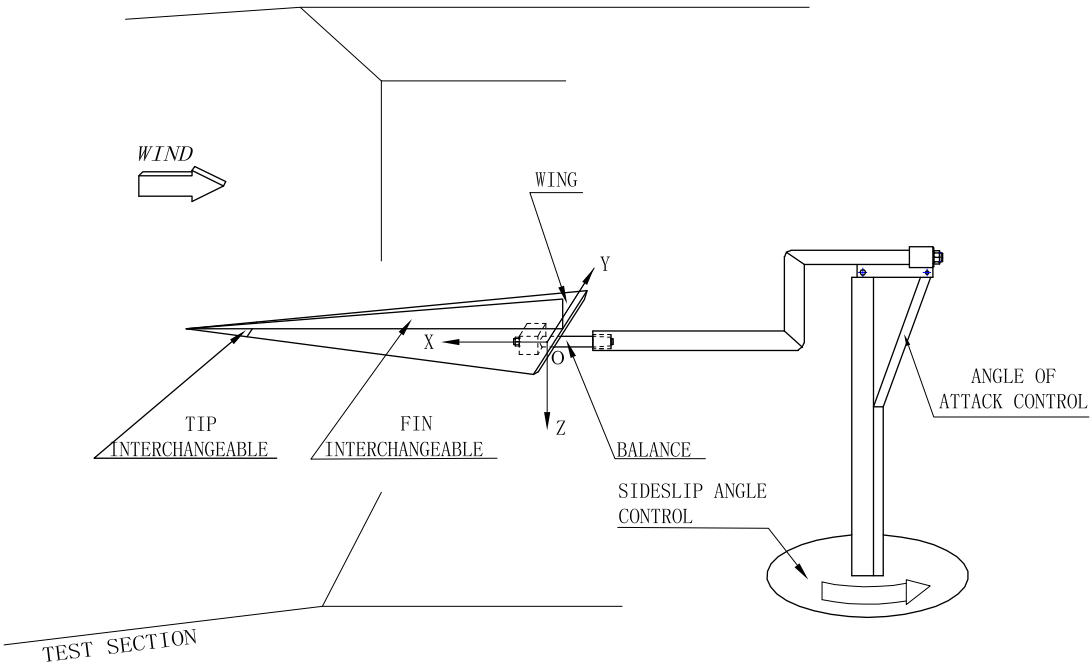

Figure 5. The test section layout.

V. Experimental Results

All tests are performed at two wind speeds, 25 m/s and 35 m/s. The free-stream Mach number is 0.07 and 0.1, respectively. The Reynolds numbers based on the root chord of the wing $Re = 1.66 \times 10^6$ and 2.33×10^6, respectively. The maximum test angle of attack is 32° and the sideslip angles are within ±10°. The aerodynamic interferences produced by the wind tunnel wall and the model support system are small and not considered. The slight deviation of angle of attack and sideslip angle due to the elastic deformation of the strain-gage balance under aerodynamic load is not corrected. To study the repeatability, the force measurements at zero sideslip are repeated for seven times for the wing model at 25 m/s wind speed and for the two wing-fin models at 35 m/s wind speed.

A. Longitudinal forces and Moment vs. α, $\beta = 0$

The longitudinal three-component data, F_X, F_Z, M_Y are originally measured and referred to the balance body system shown in Fig. 5. To facilitate a comparison with the test results of Shanks,[3] the longitudinal three-component experimental data are converted into lift, drag and pitching moment referred to the wind axes originating at the 40.0% point of the mean aerodynamic chord $\bar{c}$ of the wing. The mean aerodynamic chord of the wing $\bar{c} = 660.0\ mm$. Relative to the point of $40.0\%\bar{c}$ the pitching-moment arm of the normal force is $58.9\%\bar{c}$ and that of the tangential force is $5.46\%\bar{c}$.

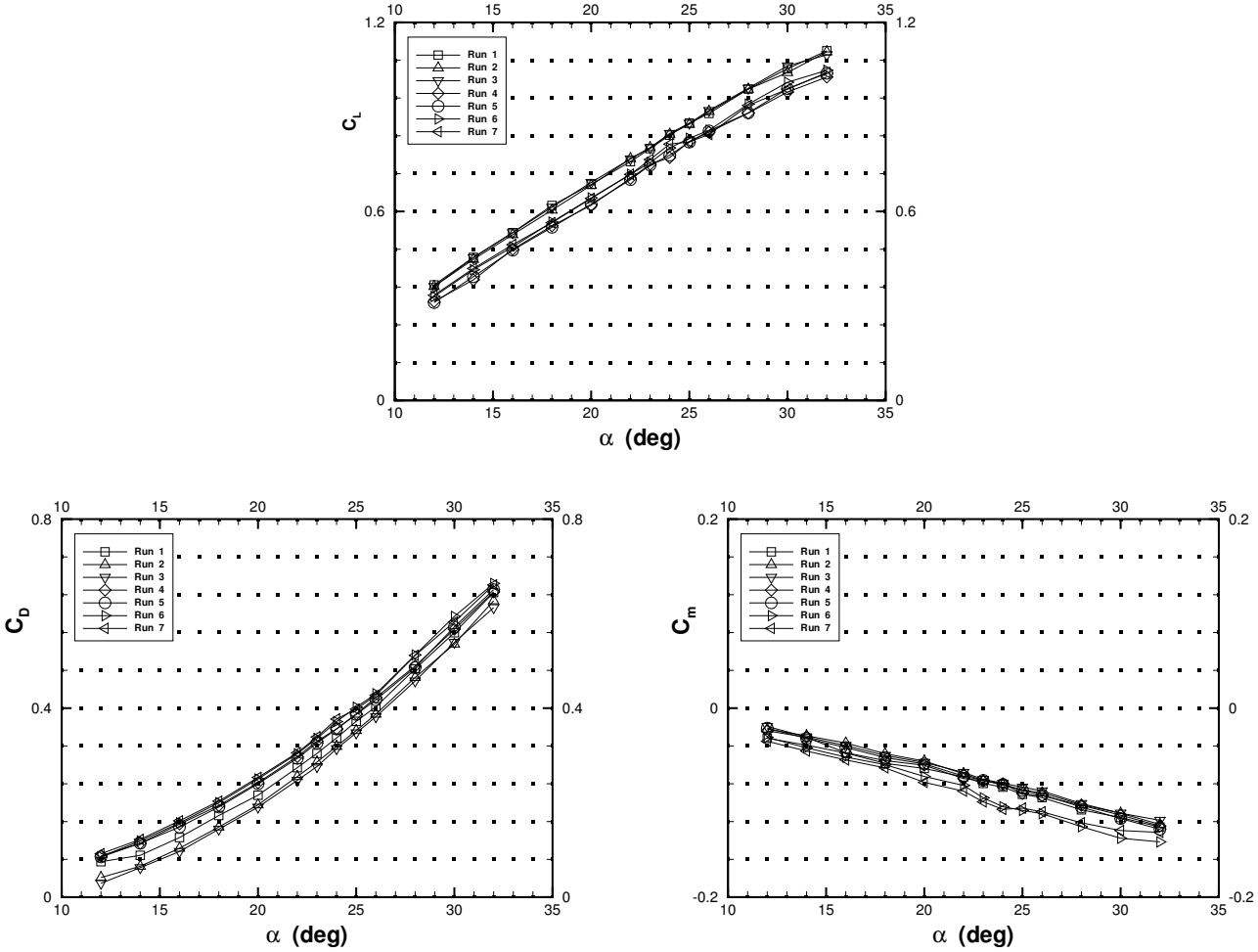

Figure 6. Lift, drag and pitching-moment coefficients for the wing model, $\beta = 0$, $Re = 1.66 \times 10^6$.

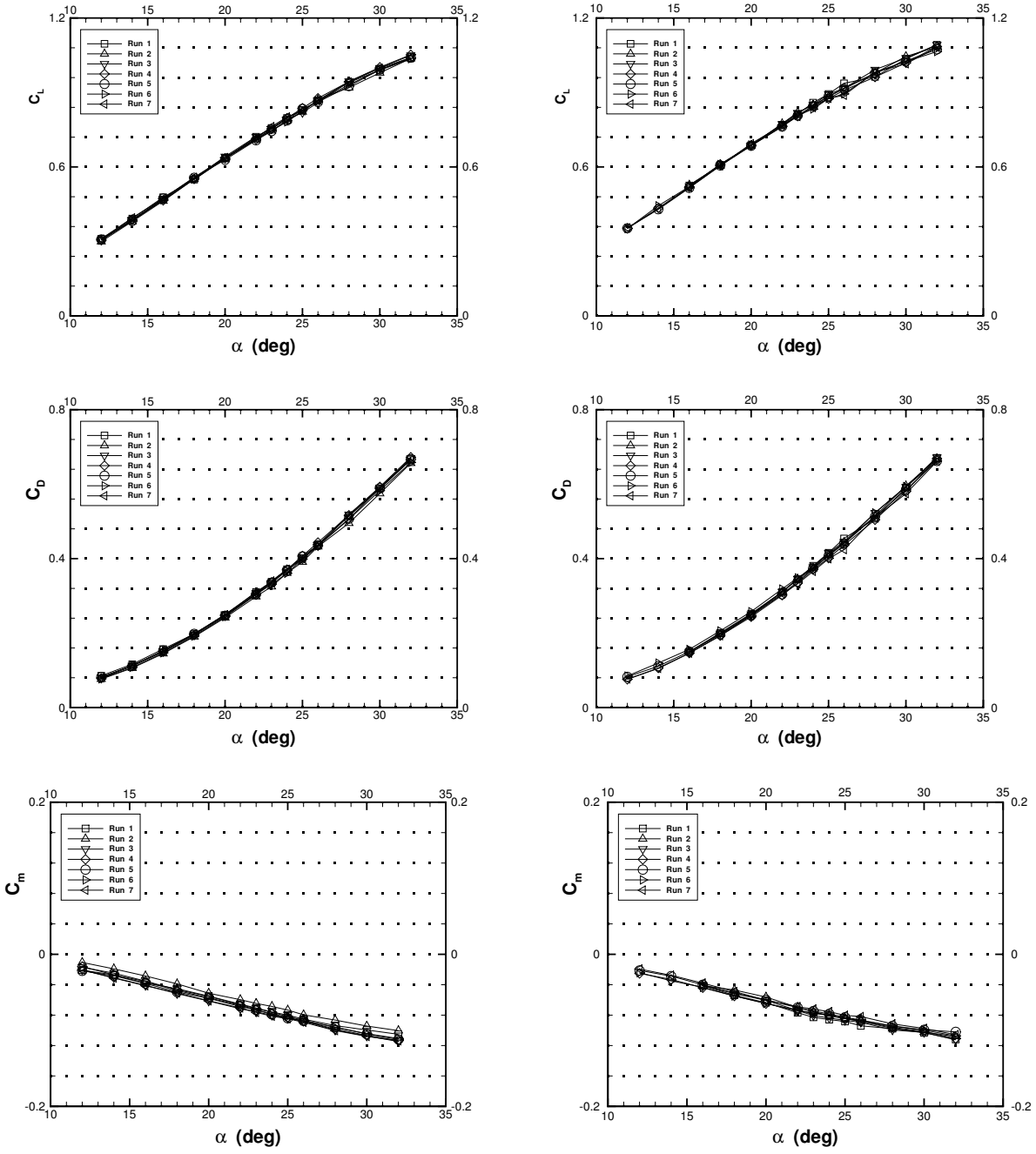

(a) Wing+0.3s-fin model

(b) Wing+0.6s-fin model

Figure 7. Lift, drag and pitching-moment coefficients, $\beta = 0$, $Re = 2.33 \times 10^6$.

The three longitudinal components of the seven repeat runs are shown in Figs. 6 and 7 for the three models. The data repeatability is estimated by reviewing the seven repeat runs and is presented in Table 4. The magnitudes of the longitudinal data repeatability are of one order greater than those of the balance uncertainty. (See Table 3.) The non-zero magnitude of the data repeatability is intrinsic to the vortex flow. It is known that the vortex has a meandering behavior although the tunnel is operating under steady conditions.[13] However, the longitudinal forces and moment can be considered steady, because the magnitude of the data repeatability is relatively small.

Table 4 Longitudinal data repeatability.

Model	C_L	C_D	C_m
Wing	± 0.02	± 0.04	± 0.02
Wing+0.3s-fin	± 0.01	± 0.005	± 0.005
Wing+0.6s-fin	± 0.01	± 0.005	± 0.005

It is seen that the data repeatability of the wing model is poor in comparison with that of the wing-fin models, because the wing model unlike the win-fin models, lacks the additional longitudinal stiffness provided by the fin.

Figure 8 presents the lift coefficient, drag coefficient and pitching-moment coefficient versus angle of attack at zero sideslip for the three models of $\epsilon = 7.5°$, $Re = 1.66 \times 10^6$ and 2.33×10^6. In case of seven repeat runs, the result lying in the mean position is chosen. A comparison with the Shanks' results[3] is included in the figure. The Shanks' wing model was a thin flat plate with round leading edge and a semi-apex angle of 8° and had a fuselage-shaped fairing to accommodate the balances on the upper surface. Shanks' test was performed at $Re = 2.05 \times 10^6$. Fig. 8 shows that C_L of the present wing+0.6s fin model is nearly equal to that of the Shanks' wing. C_D of the wing+0.6s-fin model is larger than that of all other models, since it has the largest skin area. C_m of the present three models are lower than that of the Shanks' wing. The aerodynamic center of the present models and the Shanks' model is $50\%\bar{c}$ and $45\%\bar{c}$, respectively. The deviation in C_m may be caused by the different locations of the attached internal balances between the two models. Though there are some geometric differences between the present models and the Shanks', their longitudinal forces and moment referred to the same coordinate system are nearly the same. The good agreement in the longitudinal three components provides a verification for the present test data. It is seen from Fig. 8 that the Reynolds number tested in the present study has little effect on the longitudinal three components.

It is noted that the lift lines, $C_L(\alpha)$ in Fig. 8 are nearly straight up to $\alpha = 32°$ considered. It indicates that no vortex breakdown appears on the wing in the present test. This indication is supported by others' work. Shanks[3] showed that the maximum lift coefficient occurs at $\alpha = 35° \sim 40°$ for the wing of $\epsilon = 8°$. Stahl et al.[6] for the wing of $\epsilon = 8°$ observed no vortex breakdown at the trailing edge of the wing when $\alpha = 30°$, and observed a vortex breakdown at the trailing edge when $\alpha = 35°$, at $Re = 3.4 \times 10^5$ using a smoke flow-visualization technique.

B. Lateral Force and Moments vs. α, $\beta = 0$

The measured six-component data are referred to the balance body system of axes, $OXYZ$. (See Fig. 5.) The balance body system differ from the wing body system in that the origin of the balance body system is set at the balance center rather than at the $40.0\%\bar{c}$ point of the wing. This does not affect what follows. The lateral component data of Shanks[3] were referred to the wing body system of axes originating at 40% of the mean aerodynamic chord, and were presented versus β at various α. No direct comparison with Shanks' results is made for the lateral components.

Sideslip angle is set to be zero in this subsection. Since the three models are symmetric in geometry, the lateral three components should be zero if symmetric flow remains stable, and would be non-zero when and only when the symmetric flow becomes unstable.

The original lateral three-component data at zero sideslip from the seven repeat runs are first presented and analyzed. The maximum test angle of attack is 32°, same as the longitudinal case. In this range of angle of attack, no vortex breakdown is found on the wing as shown in the study of the longitudinal data. (See Fig. 8.)

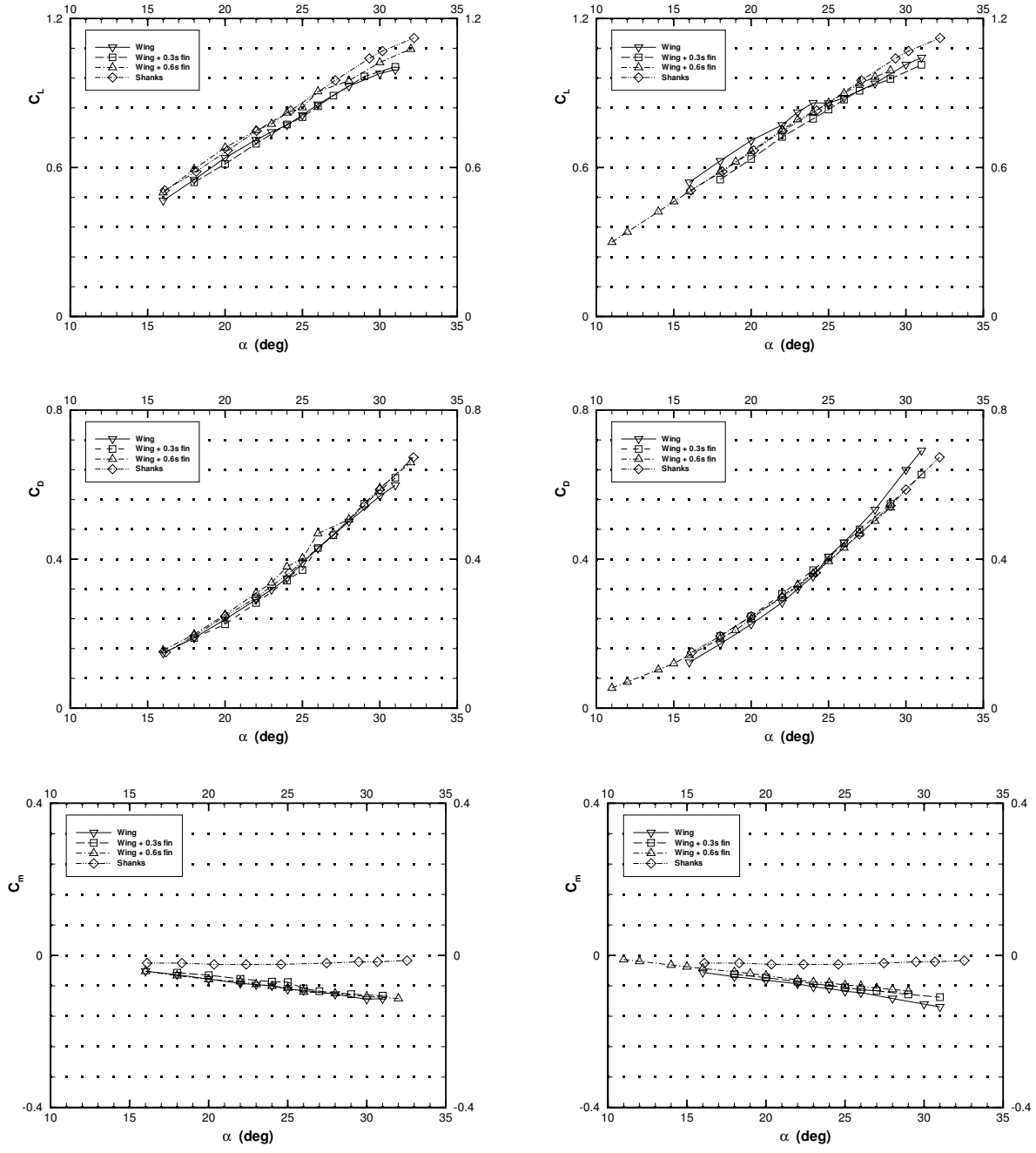

(a) $Re = 1.66 \times 10^6$

(b) $Re = 2.33 \times 10^6$

Figure 8. Lift, drag and pitching-moment coefficients for the three models compared with Shanks' results,[3] $\beta = 0$.

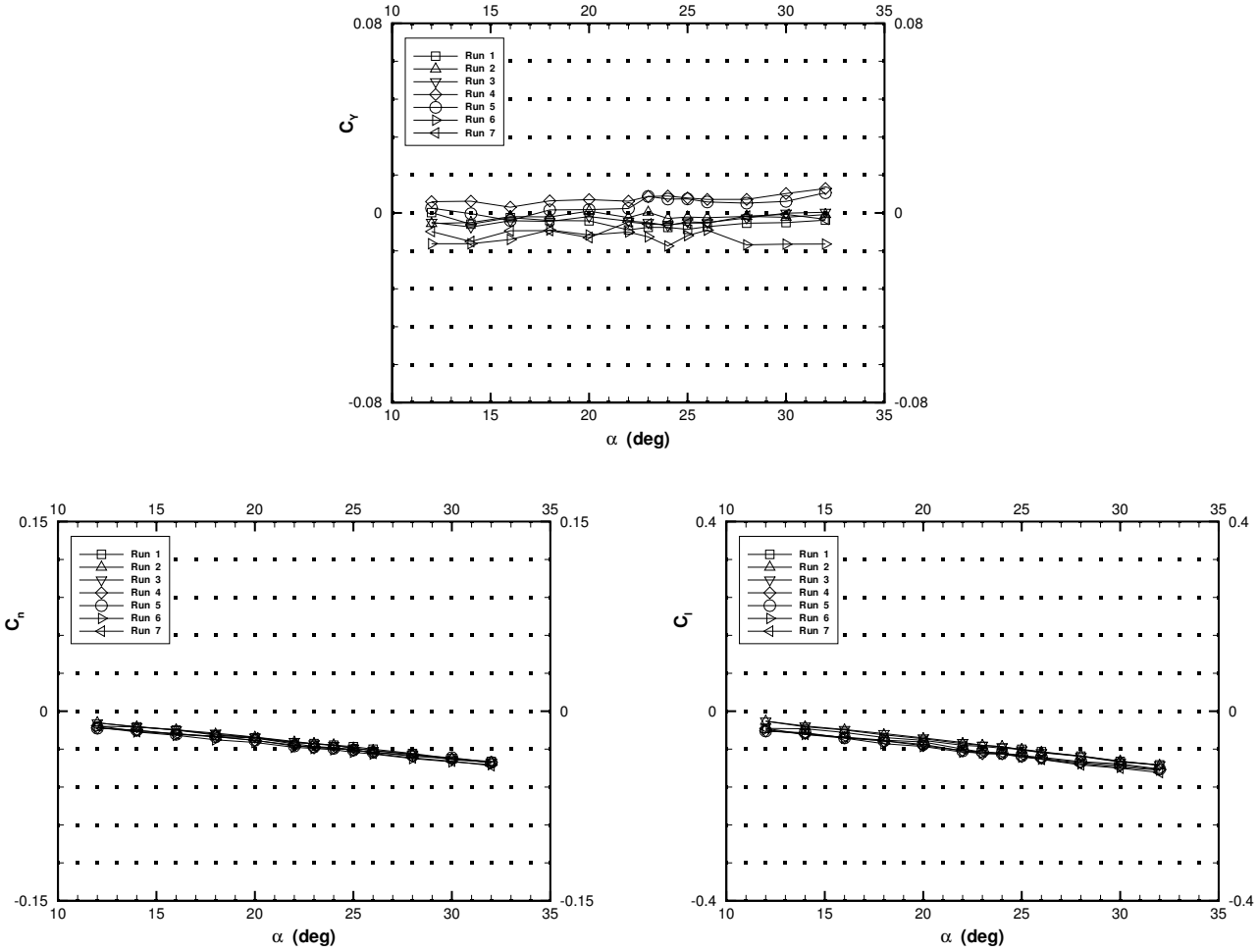

Figure 9. Side-force, yawing-moment and rolling-moment coefficients for the wing model, $\beta = 0$, $Re = 1.66 \times 10^6$.

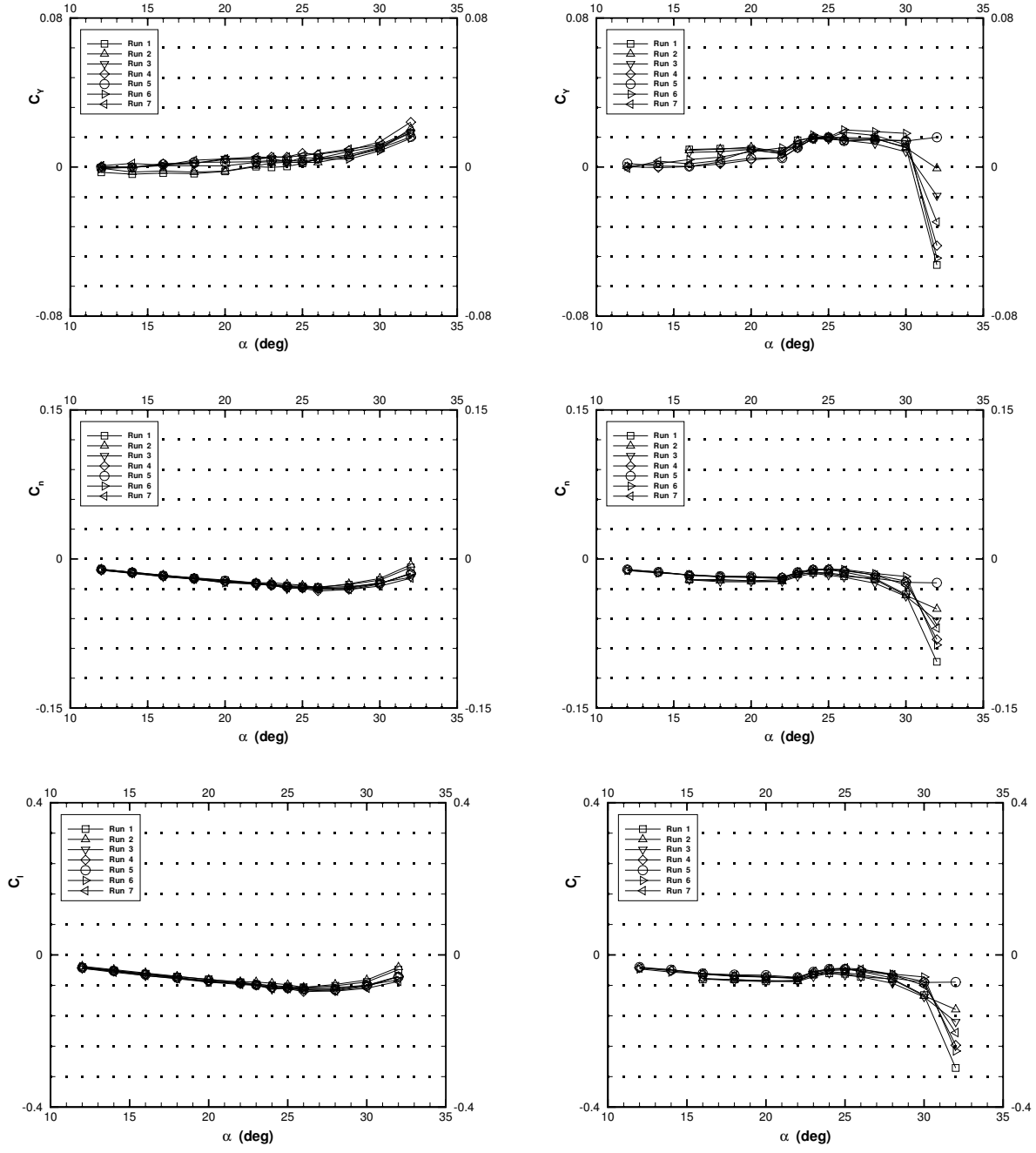

(a) Wing+0.3s-fin model

(b) Wing+0.6s-fin model

Figure 10. Side-force, yawing-moment and rolling-moment coefficients, $\beta = 0$, $Re = 2.33 \times 10^6$.

Figures 9 and 10 present the results of the seven repeat runs for the side-force, yawing-moment and rolling-moment coefficients versus angle of attack at zero sideslip for the wing model at $Re = 1.66 \times 10^6$ and for the wing+0.3s-fin model and wing+0.6s-fin model at $Re = 2.33 \times 10^6$, respectively. It is seen that the repeatability for the side force coefficient $C_Y(\alpha)$ is poor in comparison with the other two lateral components, $C_n(\alpha)$ and $C_l(\alpha)$. In order to avoid a transfer of the poor repeatability of the side force to the other lateral components, the lateral data are not converted to the conventional wing body system as stated above.

A comparison of $C_Y(\alpha)$ for the three models shows an important difference between them. The mean value of the seven repeat-test data of the side force coefficient versus angle of attack remains nearly zero throughout the entire range of the angle of attack for the wing model. For the two wing-fin models, the mean value of C_Y is zero at low angles of attack but becomes non-zero starting from a certain high angle of attack. It is seen from Fig. 10 that the wing+0.3s-fin model experiences a force-asymmetry onset at $\alpha = 26°$, the wing+0.6s-fin model experiences a force-asymmetry onset at $\alpha = 22°$. Moreover, for the wing+0.6s-fin model the data of $C_Y(\alpha)$ start to be switched to opposite sign and become erratic with growing magnitude at a further high angle of attack of $\alpha = 30°$. The data are no more repeatable, and the side force can no longer be considered steady. Thus, the wing+0.6s-fin model induces a force-unsteadiness onset at $\alpha = 30°$. Similar features are observed for both $C_n(\alpha)$ and $C_l(\alpha)$. It is important to note that throughout the entire range of the angle of attack, the lift coefficient $C_L(\alpha)$ remains nearly a straight line without vortex breakdown on the wing.

However, unlike $C_Y(\alpha)$, $C_n(\alpha)$ and $C_l(\alpha)$ do not remain zero as α is increased from zero, for the wing model. Their curve is nearly a straight line passing through the origin with a negative (non-zero) slope. For the two wing-fin models, $C_n(\alpha)$ and $C_l(\alpha)$ are also non-zero before the side-force-asymmetry onsets. It is noted that the straight line portion of $C_n(\alpha)$ for the two wing-fin models is nearly coincided with each another and also with that of the wing model, and the straight line portion of $C_l(\alpha)$ for the the two wing-fin models is also nearly coincided with that of the wing model. Evidently, there exists an interference of the normal force with the two lateral moments. The interference may be caused by an inaccuracy in the experimental setup of the model and balance combination. In the present experimental setup, the symmetry plane of the wing may not exactly coincide with the balance coordinate plane XOZ. Thus, the normal force which lies in the symmetry plane of the wing may not lie exactly in the balance plane XOZ, and produce an interfering lateral moments about the balance axes OZ and OX. Since the model and balance combination setup is common in the three models and the normal forces are nearly equal for the three models at the same angle of attack, the interfering lateral moments are almost the same for the three models at a given angle of attack.

The interference of the normal force to $C_n(\alpha)$ can be eliminated by the following steps:

1. Calculate the dimensionless yawing-moment arm for the normal force based on the wing span b

$$\kappa_n(\alpha) = C_n(\alpha)/C_N(\alpha), \tag{1}$$

   where $C_n(\alpha)$ and $C_N(\alpha)$ are read from the original-measurement data;

2. Determine the symmetry-flow range of α before asymmetry onset, if any;

3. Take the average of κ_n over the symmetry-flow range of α to obtain $\overline{\kappa_n}$;

4. The *corrected* $C_n(\alpha)$ over the entire range of α is obtained as follows,

$$Corrected\,[C_n(\alpha)] = C_n(\alpha) - C_N(\alpha)\overline{\kappa_n}. \tag{2}$$

Table 5 Dimensionless moment arms κ_n and κ_l.

α	$-\kappa_n$			$-\kappa_l$		
	Wing	Wing+0.3s-fin	Wing+0.6s-fin	Wing	Wing+0.3s-fin	Wing+0.6s-fin
12°	0.031863	0.032512	N/A	0.097090	0.101811	N/A
14°	0.026794	0.032702	N/A	0.080183	0.100114	N/A
16°	0.027315	0.032710	0.035891	0.082141	0.098686	0.110786
18°	0.029369	0.032515	0.032282	0.086494	0.097922	0.100606
20°	0.029334	0.031209	0.029987	0.085620	0.094477	0.094839
22°	0.031063	0.030623	0.025138	0.089407	0.091852	0.080343
23°	0.029977	0.031161	0.017417	0.087022	0.093945	0.058948
24°	0.029618	0.030671	0.014994	0.086126	0.091941	0.051458
25°	0.029378	0.029851	0.014794	0.084085	0.090257	0.050349
26°	0.030200	0.029046	0.016787	0.085851	0.087757	0.055169
28°	0.030423	0.024086	0.018142	0.086177	0.075897	0.058129
30°	0.031447	0.018487	0.029857	0.088780	0.061861	0.088669
32°	0.031029	0.006795	0.008760	0.088258	0.031434	0.231913

Similar procedures are used to correct the measured $C_l(\alpha)$, where a dimensionless rolling-moment arm for the normal force based on b, $\kappa_l(\alpha) = C_l(\alpha)/C_N(\alpha)$ and its average over the symmetry-flow range of α, $\overline{\kappa_l}$ are introduced. As an example, the correction for the run-one data is presented. Table 5 gives the dimensionless moment arms, κ_n and κ_l versus α based on the wing span b for the three models, where N/A denotes not available because of no test is conducted at this angle of attack, and the underlined number denotes the appearance of sharp change for κ_n and κ_l at this angle of attack.

The sharp change of the dimensionless moment arms marked by the underline in Table 5 shows that at this angle of attack, besides the interfering lateral moments a real non-zero lateral moments acting on the model start to appear, i.e., a force-asymmetry onset occurs. From examining the magnitude of κ_n and κ_l versus α in Table 5, it is found again that the wing+0.3s-fin model experiences a force-asymmetry onset at $\alpha = 26°$ and the wing+0.6s-fin model experiences a force-asymmetry onset at $\alpha = 22°$, while the wing alone experiences no force asymmetry. The exact force-asymmetry-onset angle-of-attack is obviously a matter of experimental judgment. However, it is fairly clear in the present investigation. It is seen that the dimensionless yawing-moment arms is nearly a constant of -0.03 and the dimensionless rolling-moment arms is nearly a constant of -0.1 for all three models at all angles of attack before force asymmetry onsets, if any. This is due to the fact that the three models share the common experimental setup of the wing-balance combination. The rest of the seven repeat tests have the same features.

According to the steps listed above, the *corrected* yawing-moment and rolling-moment coefficients of the seven repeat runs versus angle of attack at zero sideslip for the wing model at $Re = 1.66 \times 10^6$, wing+0.3s-fin model and wing+0.6s-fin model at $Re = 2.33 \times 10^6$ are calculated and shown in Fig. 11. Now, same as the side force of the original experimental data shown in Figs. 9 and 10, the *corrected* lateral moments C_n and C_l are nearly zero over the entire range of α for the wing model, and remain zero before the force asymmetry onsets for the two wing-fin models. The above correction method may be considered justified.

The lateral three-component data are repeatable before force unsteadiness onsets. Table 6 gives the lateral-data repeatability for the three models before force unsteadiness onsets. The magnitude of the lateral-data repeatability is greater than the magnitude of the balance uncertainty by one order of magnitude (See Table 3) and is caused by the intrinsic meandering behavior of the vortex flow. However, the magnitude of the lateral-data repeatability is small in comparison with the lateral data themselves after the force asymmetry onsets, and thus, the force can be considered as steady until the force unsteadiness onsets. The wing model has poor repeatability in comparison with the two wing-fin models, because the wing alone has less longitudinal stiffness. Moreover, for all the three models, the side force has poor repeatability in comparison with the other two lateral components.

Table 6 Lateral data repeatability before force-unsteadiness onset.

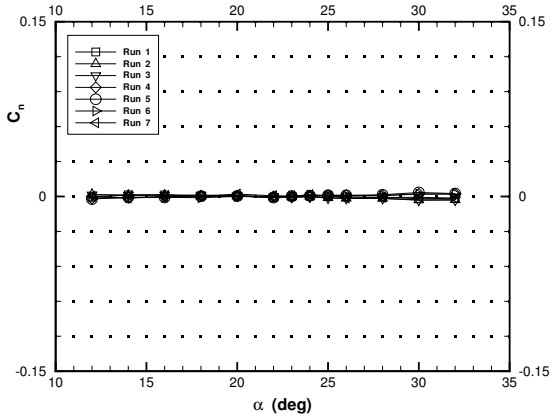

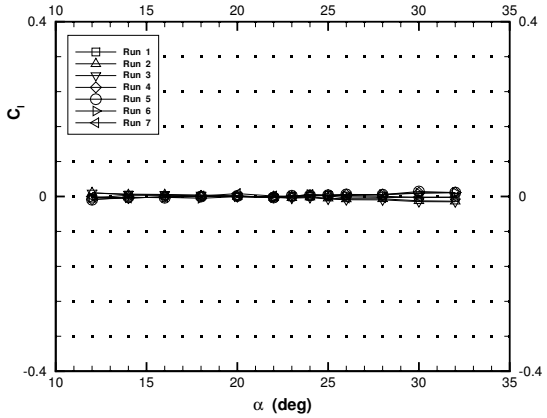

(a) Wing model, $Re = 1.66 \times 10^6$

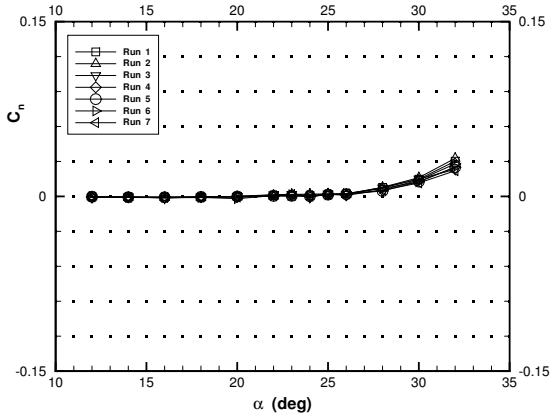

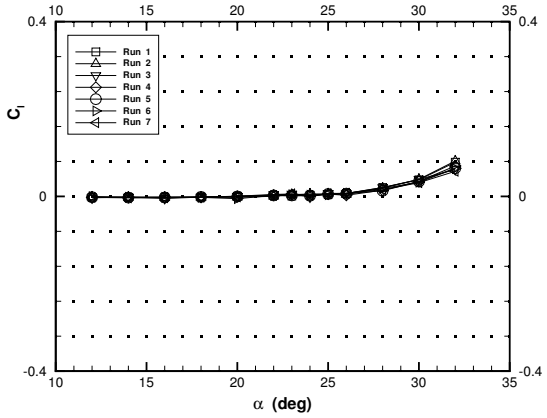

(b) Wing+0.3s-fin model, $Re = 2.33 \times 10^6$

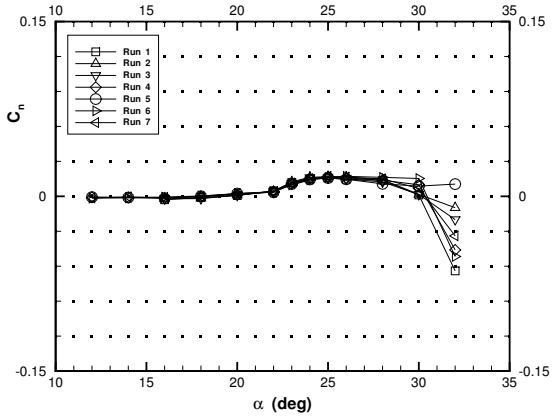

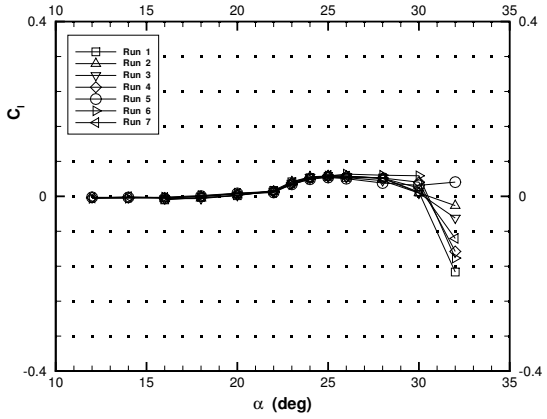

(c) Wing+0.6s-fin model, $Re = 2.33 \times 10^6$

Figure 11. *Corrected* **yawing-moment and rolling-moment coefficients,** $\beta = 0$**.**

Model	C_Y	C_n	C_l
Wing	± 0.01	± 0.005	± 0.01
Wing+0.3s-fin	± 0.005	± 0.001	± 0.002
Wing+0.6s-fin	± 0.005	± 0.001	± 0.002

It is noted that after force-asymmetry onset, the three lateral components in every repeat run share the same sign. The side force and the yawing moment for the wing-fin models are mainly produced by the fin and they have the same sign. The rolling moment is produced by both the fin and the wing and their contributions have the opposite sign. In the present cases, the fin has larger contribution and, thus, the rolling moment shares the same sign with the side force. The sign variation of the three lateral components versus angle of attack for the wing-fin models is consistent with one another in consideration of that they are referred to the balance body system originating at the balance center. For example, if C_Y is changed from positive to negative at certain angle of attack, so are C_n and C_l at the same angle of attack.

Asymmetry onset for a symmetric body at zero sideslip is a bifurcation phenomenon. There exists an another solution mirror-imaged to the present solution. In the present tests, the three lateral components C_Y, C_n and C_l for the wing-fin models at the force asymmetry onset, all change from zero to positive as the angle of attack is increased. The change can be in the opposite direction. Which solution of the bifurcation occurs is determined by the slight asymmetric disturbances existing in the experimental setup and the free-stream flow.

C. Lateral Force and Moments Induced by Fin vs. β

In this subsection, the force-asymmetry onset of the wing-fin models is investigated experimentally by another method. The variation of the three lateral components versus angle of sideslip at a series of angle of attack are measured by the six-component internal strain-gage balance. The test range of the sideslip is from -10° to 10° with an increment of 2°. The test range of the angle of attack is same as above. Only yawing and rolling moments are considered. Since their repeatability is good, no repeat tests are conducted for this investigation. The curve of each lateral component versus sideslip at constant angle of attack is nearly a straight line in the vicinity of zero sideslip and thus, provides a credible value for the lateral component at zero sideslip and various angles of attack.

As shown in the last subsection, there exists an interference of the normal force with the yawing and rolling moments about the balance coordinate axes in the present experimental setup. The interfering yawing moments for the three models are nearly equal at a given angle of attack, and the same is true for the interfering rolling moments. Thus, the interfering lateral moment for a wing-fin models at each angle of attack can be eliminated by a subtraction of the originally measured lateral moment of the wing model from the corresponding one of the wing-fin model. This subtraction results in a real increment of the lateral component due to adding the fin to the wing. In this subsection, the increment of the lateral moments produced by the fin versus sideslip angle at various angles of attack is studied instead of the lateral moments themselves. The increment of the side force is not studied because of the poor repeatability of the side force, especially for the wing model, as shown in last subsection.

Figures 12 and 13 present the increment of yawing-moment and rolling-moment coefficients produced by adding the $0.3s$-fin and $0.6s$-fin to the wing, respectively. $Re = 1.66 \times 10^6$ and 2.33×10^6. Only five angles of attack and the range of $\beta = -2^\circ$ to 2° are shown in the figures for clarity. For the wing+$0.6s$-fin model, the data at $\beta = \pm 2^\circ$ and $Re = 2.33 \times 10^6$ are missing because the appearance of strong model vibrations prohibits the measurements.

From Figs. 12 and 13, the angle of attack at which $\Delta C_n(\beta)$ and $\Delta C_l(\beta)$ at $\beta = 0$ start to be non-zero is the asymmetry-onset angle-of-attack. The results fairly confirm the force-asymmetry-onset angle-of-attack determined in last subsection. It is noted that the Reynolds numbers considered in the present tests have little effect on the results.

VI. Comparison of Experimental and Theoretical Results

The theory is a linear analysis. It predicts instability onset of the *stationary* symmetric vortex pair over the wing alone model and the two wing-fin models under small perturbations in Section III. The force-

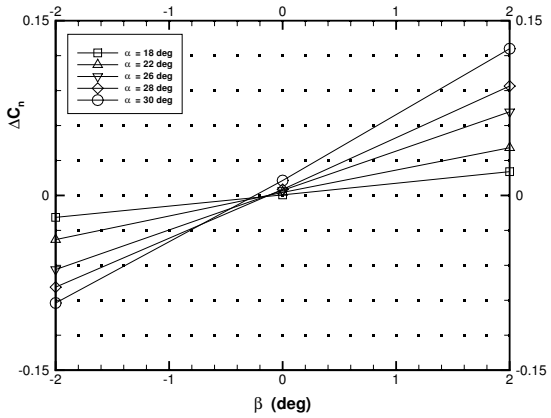

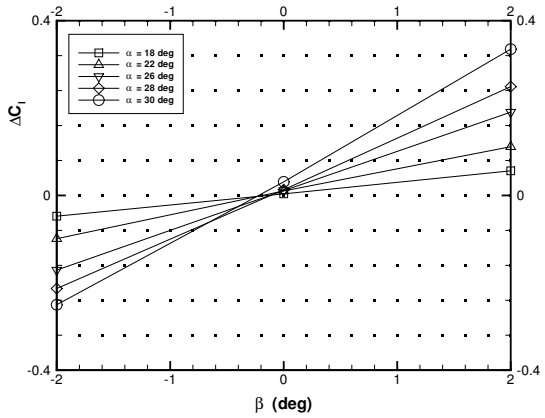

(a) $Re = 1.66 \times 10^6$

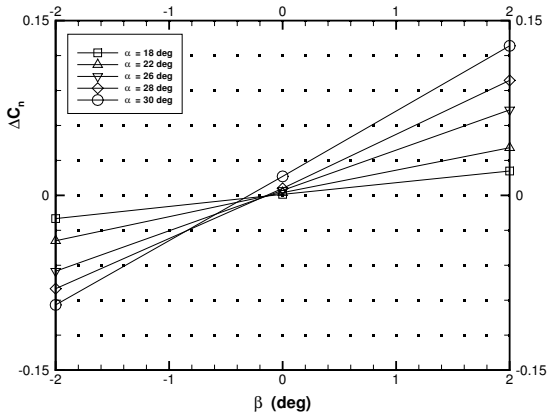

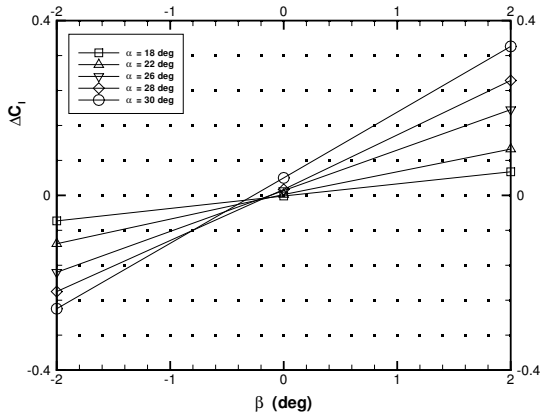

(b) $Re = 2.33 \times 10^6$

Figure 12. Yawing- and rolling-moment coefficients induced by $0.3s$-fin.

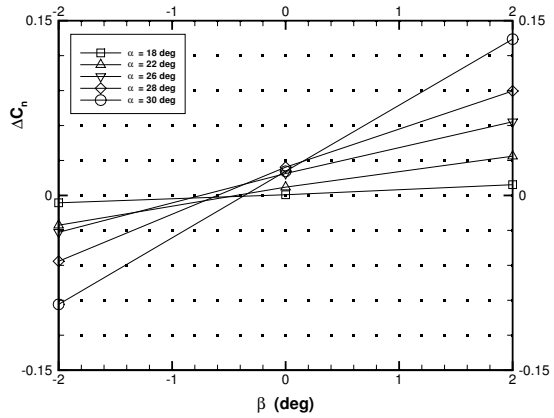

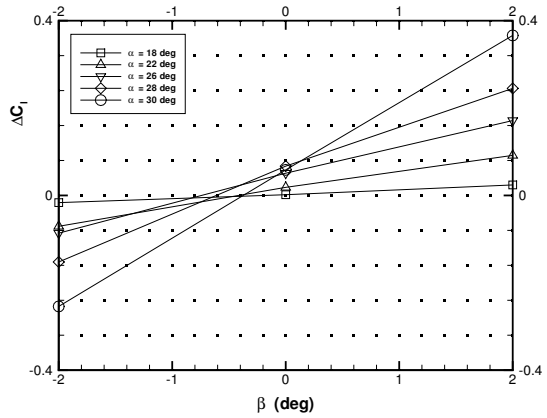

(a) $Re = 1.66 \times 10^6$

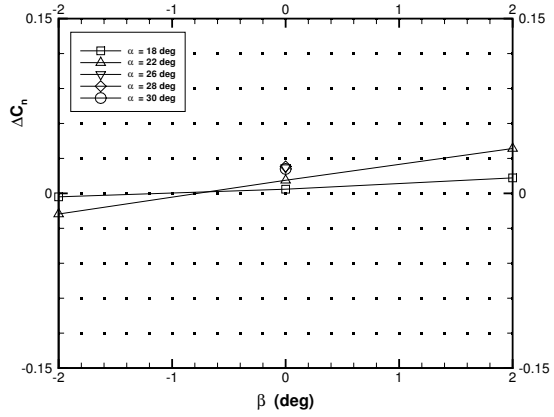

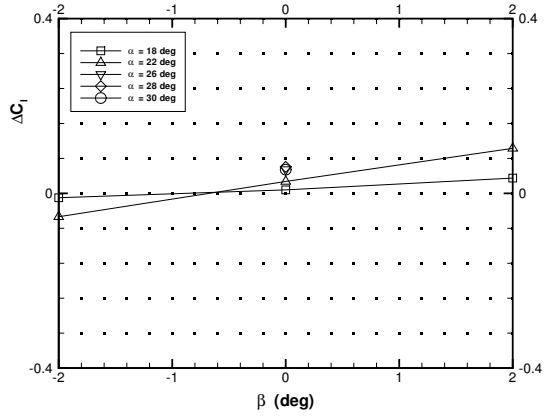

(b) $Re = 2.33 \times 10^6$

Figure 13. Yawing- and rolling-moment coefficients induced by $0.6s$-fin.

asymmetry onset for the two wing-fin models found in this experiments clearly indicates that the vortex pair separated from the leading edge of the wing can no longer be symmetric and has to be changed from symmetric to asymmetric. Therefore, the force-asymmetry-onset angle-of-attack observed by the present experiments could be comparable with the instability-onset angle-of-attack predicted by the theory.

The experimental results of the angles of attack for force-asymmetry onset and force-unsteadiness onset (if any) for the three models at zero sideslip are summarized in Table 7, where No denotes no onset and N/A denotes not available due to the limited range of the test angle of attack. The theoretical predictions from Table 1 are included in Table 7 for comparison. The experimental force-asymmetry-onset angle-of-attack and the theoretical instability-onset angle-of-attack are in good qualitative agreement, but significantly different in magnitude. The result of the original theory are consistently lower than that of the experiment, whereas that of the modified theory are consistently higher than that of experiment. The quantitative disagreement may be attributed to the simplifications made in the theoretical model for the mathematical analysis.

Table 7 Experimental angle-of-attack for force-asymmetry and force-unsteadiness onset compared with theoretical angle-of-attack for instability onset.

Model	Experimental		Theoretical	
	Asymmetry onset	Unsteadiness onset	Original	Modified
Wing	No	No	No	No
Wing+0.3s-fin	26°	N/A	23°	34°
Wing+0.6s-fin	22°	30°	18°	27°

Besides predicting instability onset, the theory predicts that there exists an angle of attack below which the two dorsal fins considered have no effect at all on the stability of the *stationary* symmetric vortex pair over the original wing. This angle of attack is 20° from the modified theory. This is verified since the experimental force-asymmetry-onset angle-of-attack for the two wing-fin models is greater than 20°.

Using a smoke-laser-sheet visualization technique, Meng et al.[8] studied the vortex flow over a sharp-edged flat-plate delta wing having the same semi-apex angle as the present model with a dorsal fin of height $0.75s$ or $1.50s$ at a fixed angle of attack of $\alpha = 29.02°$ and $\beta = 0$. It was observed that the vortex flow over the wing-alone model and the wing+$1.50s$-fin model is symmetric, conical and steady; and the flow over the wing+$0.75s$-fin model is asymmetric, non-conical and unsteady. No visualization study is conducted for the present wing-fin models. However, based on the observations of Ref. 8, it is conjectured that the vortex flow over the present wing+fin models at zero sideslip remains symmetric, conical and steady at angles of attack before the force-asymmetry onset; becomes asymmetric and/or non-conical but still steady at angles of attack between the force-asymmetry onset and force-unsteadiness onset; and becomes asymmetric, non-conical and unsteady at angles of attack after the force-unsteadiness onset.

VII. Conclusions

The measurements using a six-component internal strain-gage balance show that when a flat-plate dorsal fin of low height is added in the symmetry plane of a 82.5 degrees swept and sharp-edged flat-plate delta wing, an asymmetry onset in force occurs at a high angle of attack and zero sideslip, whereas no force-asymmetry onset is found for the wing-alone model in the same test range of angle of attack up to 32 degrees. Two fin heights are tested. The ratios of the local fin height to the local semi-span are 0.3 and 0.6, respectively. The higher the fin is, the lower the angle of attack at which the force asymmetry occurs is. These experimental findings clearly validate the predictions of the instability of the *stationary* symmetric vortex pair over slender conical wing-fin model by the theory of Cai et al. (J. of Fluid Mech., vol. 480, 2003, pp. 65-94).

As angle of attack is increased beyond that of force-asymmetry onset, the measurements depict that a force-unsteadiness onset occurs before vortex breakdown reaches the wing for wing-fin model. Beyond the angle of attack of the force-unsteadiness onset, the lateral three components become erratic and switch to opposite sign with growing magnitude. This force development is believed to be caused by an asymmetric, non-conical and oscillating disposition of vortices off the sharp leading edges of the wing at zero sideslip.

The measured longitudinal-components versus angle of attack at zero sideslip agree well with the data of Shanks (1963). The angles of attack for force-asymmetry onset and force-unsteadiness onset (if any) are determined by analyzing the measured lateral-components versus angle of attack at zero sideslip and

verified by studying the increment of the measured yawing- and rolling-moments due to fin versus sideslip angle at various angles of attack. The experimental and theoretical results of the angles of attack for the force-asymmetry, or instability onset versus the fin height are in good qualitative agreement but significantly different in magnitude. The quantitative difference may be attributed to the simplifications made in the theory.

The measured longitudinal-components are repeatable and steady in the entire range of the test angle of attack at zero sideslip for the wing and wing-fin models, and so are the measured lateral-components for the wing model but not so for the wing-fin models. For the wing-fin models, the measured lateral-components are repeatable and steady only when angle of attack is below that for force-unsteadiness onset. The angle of attack for the force-asymmetry onset and force-unsteadiness onset is independent of the test Reynolds number ($1.66 \times 10^6 \sim 2.33 \times 10^6$ based on the root chord of the wing).

The paper provides by the first time direct force-measurement evidence of the theoretical predictions and confirmation that the absolute-type instability studied by the theory could be the origin of asymmetry of vortices over slender conical fore-bodies, and depicts the development of force-unsteadiness onset with increase of angle of attack at zero sideslip after force-asymmetry onset but before vortex breakdown on a wing-fin model.

Acknowledgments

The first author wishes to acknowledge support by the Doctorate Innovation Foundation of Northwestern Polytechnical University through Grant CX200501. The authors would like to express their gratitude to Yongwei Gao, Zhongxiang Xi, Zenghong Xi, and Chunsheng Xiao in Northwestern Polytechnical University for their valuable technical guidance and support in the wind-tunnel tests, to Jinsheng Cai of National University of Singapore for providing new unpublished theoretical results, and to Shuchi Yang from the University of California, Irvine, for his various help with this research and the preparation of this paper. Thanks are also to Jiangnan Hao and other people who helped make the test models.

References

[1]Ericsson, L., "Sources of high alpha vortex asymmetry at zero sideslip," *Journal of Aircraft*, Vol. 29, 1992, pp. 1086–1090.

[2]Lowson, M. and Ponton, A., "Symmetry breaking in vortex flows on conical bodies," *AIAA Journal*, Vol. 30, 1992, pp. 1576–1583.

[3]Shanks, R., "Low-subsonic measurements of static and dynamic stability derivatives of six flat-plate wing having leading-edge sweep angles of 70° to 84°," NASA TN D-1822, 1963.

[4]Polhamus, E., "Predictions of vortex-lift characteristics by a leading-edge suction analogy," *Journal of Aircraft*, Vol. 8, 1971, pp. 193–199.

[5]Keener, E. and Chapman, G., "Similarity in vortex asymmetries over slender bodies and wings," *AIAA Journal*, Vol. 15, 1977, pp. 1370–1372.

[6]Stahl, W., Mahmood, M., and Asghar, A., "Experimental investigations of the vortex flow on delta wings at high incidence," *AIAA Journal*, Vol. 30, 1992, pp. 1027–1032.

[7]Cai, J., Liu, F., and Luo, S., "Stability of symmetric vortices in two-dimensions and over three-dimensional slender conical bodies," *J. Fluid Mech.*, Vol. 480, April 2003, pp. 65–94.

[8]Meng, X., Qiao, Z., Gao, C., Luo, S., and Liu, F., "Visualization of Vortex Flow over Delta Wing with Dorsal Fin," AIAA Paper 2005-1058, June 2005.

[9]Cai, J., Tsai, H.-M., Liu, F., and Luo, S., "Vortex core and its effects on the stability of vortex flow over slender conical bodies," AIAA Paper 2005-0062, Jan. 2005.

[10]Legendre, R., "Écoulement au Voisinage De La Pointe aAvant D'une Aile A forte Fléche Aux Incidences Moyennes," *La Recherche Aeronautique, Bulletin Bimestriel, De L'Office National D'Études Et De Recherches Aeronautiques*, Jan.-Feb. 1953.

[11]Sychev, V., "Three-dimensional hypersonic gas flow past slender bodies at high angle of attack," *Journal of Maths and Mech. (USSR)*, Vol. 24, 1960, pp. 296–306.

[12]Cai, J., Luo, S., and Liu, F., "Stability of Symmetric and Asymmetric Vortex Pairs over Slender Conical Wings and Bodies," *Physics of Fluids*, Vol. 16, No. 2, Feb. 2004, pp. 424–432.

[13]Orloff, K., "Trailing vortex wind-tunnel diagnostics with Laser velocimeter," *Journal of Aircraft*, Vol. 11, No. 8, Aug. 1983, pp. 477–482.